The Astrophysical Journal, 621:1109–1120, 2005 March 10

TRANSIENT CORONAL HOLES AS SEEN IN THE He I 1083 nm MLSO OBSERVATIONS

G. de Toma, T. E. Holzer, J. T. Burkepile, and H. R. Gilbert
High Altitude Observatory, National Center for Atmospheric Research, Boulder, CO 80301
Received 2004 August 18; accepted 2004 September 27

ABSTRACT

Observations from *Yohkoh* SXT and *SOHO* EIT have shown that dimming regions often appear on the solar disk near the location of a coronal mass ejection (CME). We now can see brightenings in He I 1083 nm observations made at the Mauna Loa Solar Observatory (MLSO) that form at the same time and are cospatial with the EUV intensity dimmings observed from space. The He I 1083 nm brightenings are induced by a decrease of the overlying coronal radiation. The EUV and X-ray dimmings and He I 1083 nm brightenings can thus be interpreted as different manifestations of the decreased coronal density caused by the ejection of coronal material during the eruption, i.e., as transient coronal holes. In this paper we present examples of transient coronal holes that form during the CME onset as seen in He I 1083 nm data and compare them with simultaneous observations in the Fe XII 19.5 nm line. We find that there is good agreement in both shape and size of the transient coronal holes at these two wavelengths. The 3 minute cadence of the He I 1083 nm observations taken at MLSO is used to determine the appearance and evolution of transient coronal holes with high temporal accuracy. Additional data in the Hα line and in broadband visible light are used to investigate the relation of transient coronal holes to the flare, filament eruption, and CME. The cases presented here illustrate how the higher time cadence of the MLSO observations can complement space data to establish the chronology of the various manifestations of solar activity associated with a CME.

Subject headings: Sun: chromosphere — Sun: corona — Sun: coronal mass ejections (CMEs) — Sun: filaments — Sun: flares

1. INTRODUCTION

Coronal mass ejections (CMEs) are large, magnetized plasma structures that are ejected from the solar corona into the heliosphere (Hundhausen 1997, 1999). CMEs can cause interplanetary shocks and drive geomagnetic disturbances and are one of the most important sources of space weather. Despite the extensive observational and theoretical research on CMEs, the origin and early development of these solar disturbances are still not well understood. CMEs usually involve a large-scale reconfiguration of the solar corona and are associated with many other forms of solar activity (see, e.g., the review papers of Webb 2000; Gopalswamy & Thompson 2000; Hudson & Cliver 2001; Plunkett et al. 2001 and references therein). Manifestations of surface activity occurring at the time of CMEs include filament eruptions, flares (in the form of Hα two-ribbon flares, EUV post-eruption loops, and bright X-ray arcades), waves, and transient coronal holes. It is the last phenomenon and its appearance at different wavelengths that are of special interest to us in this study.

Transient coronal holes are dim regions in EUV and X-ray observations appearing suddenly on the solar disk near the location of a CME. They typically form in less than 1 hr and slowly fade in 1–2 days, have intensity contrast similar to other coronal holes, and usually overlie predominantly unipolar magnetic field regions in the photosphere. At times, a pair of holes forms on the opposite sides of a neutral line, but other times only one hole is clearly visible (Hudson & Webb 1997; Thompson et al. 1998; Kahler & Hudson 2001). The shape of transient holes can vary significantly from almost symmetric, compact lobes near the source region of the CME to regions with fairly irregular shape and a more diffuse appearance that can extend to significant distance from the CME source region (Thompson et al. 1998, 2000).

Transient coronal holes were first detected as rapid decreases in intensity or "coronal depletions" in coronagraph images (Hansen et al. 1974) and in *Skylab* data as areas of reduced soft X-ray emission identified as "X-ray voids" (Rust & Hildner 1976; Webb et al. 1978; Rust 1983). They have been extensively studied in X-ray with *Yohkoh* SXT observations (Watanabe et al. 1994; Manoharan et al. 1996; Hudson et al. 1996, 1998; Sterling & Hudson 1997; Hudson & Webb 1997; Gopalswamy & Hanaoka 1998; Sterling et al. 2000; Kahler & Hudson 2001). The first dimmings identified in X-ray observations did not have sufficient overlap with white-light coronal observations to definitively connect dimmings with CMEs, yet they were interpreted as low corona signatures of CMEs (Rust 1983). This interpretation was confirmed by subsequent observations (Sterling & Hudson 1997; Gopalswamy & Hanaoka 1998). A decrease in coronal brightness can be caused by a density decrease or by a temperature variation of the emitting plasma. The timescale over which dimmings develop is typically 1 hr, much faster than the radiative cooling time (Hudson et al. 1996). Thus, the rapid appearance of the dimmings suggests that they are due to density depletions. It was speculated that dimmings were created when coronal material was evacuated during the expulsion of a CME and suggested that the dimming regions represented at least some of the mass expelled in the CME itself.

Zarro et al. (1999) analyzed a CME event where the EUV dimmings occurred at the same location as the X-ray dimmings, previously identified by Sterling & Hudson (1997). More events of this kind were reported in a later study by Sterling et al. (2000). The observations of almost simultaneous and cospatial dimmings at all the EUV wavelengths covered by the EIT instrument and in X-ray supported the previous interpretation that dimming regions are produced by a density depletion rather than by a temperature variation (Thompson et al. 1998). This has been confirmed by observations at the limb made with the CDS instrument, which has the ability to observe several emission lines simultaneously covering the temperature range from 20,000 to about 2×10^6 K (Harrison & Lyons 2000; Harrison et al. 2003; Howard & Harrison 2004). Furthermore, in one case, CDS observations (Harra & Sterling 2001) have shown that

the areas of coronal dimmings corresponded to outflowing material. There is, thus, strong observational evidence supporting the idea that transient coronal holes are associated with mass loss. How this density depletion occurs and how much of the CME mass can be accounted for by the dimming regions in EUV and X-ray is not completely clear. A density depletion above the dimming regions could be caused by the ejection of coronal plasma along field lines opened during the CME or by a fast expansion of the plasma volume above the dimming regions (Gibson & Low 2000; Mandrini et al. 2005). If previously closed magnetic field lines temporarily open to the interplanetary space in the regions of transient coronal holes, they can provide a temporary source of high-speed solar wind that can persist for up to 2–3 days after the CME (C. Arge et al. 2005, in preparation). Several estimates of the mass associated with transient coronal holes have been made (Hudson et al. 1996; Hudson & Webb 1997; Sterling & Hudson 1997; Gopalswamy & Hanaoka 1998) and for specific events compared to the mass of the associated CME (Harrison & Lyons 2000; Neupert et al. 2001; Harrison et al. 2003). Mass estimates of transient coronal holes based on *SOHO* EIT and *Yohkoh* SXT are usually lower than the typical CME mass. The analysis of Harrison et al. (2003) of five limb dimmings detected with the *SOHO* CDS instrument gives mass-loss estimates for the dimming regions comparable or larger to the mass of the overlying CME, indicating that, for these cases, a large fraction of the CME mass originated in the low corona. We note that all these calculations depend on the assumed emission measure distribution, which is not well known, and also that such estimates tend to be lower limits because of the possible superposition of brighter parts of the flaring region along the line of sight.

The numerous EUV observations of transient coronal holes made with the instruments on *SOHO* have shown that coronal dimmings on the disk (Thompson et al. 1998; Zarro et al. 1999; Delannée et al. 2000) or at the limb (Dere et al. 1997; Delannée et al. 2000; Neupert et al. 2001; Harrison et al. 2003; Howard & Harrison 2004) are relatively common events during CMEs and are also associated with filament eruptions, flares, and coronal wave transients. Since then, transient coronal holes and waves have been used as indicators of CME activity in the low corona. To understand the onset of CMEs, it is important to establish the order in which these various disk manifestations of CMEs occur and how they relate to each other. In addition, the chronology of events in the early phase of a CME provides important observational constraints to models of CME. Thompson et al. (1998) indicated that for the 1997 May 12 CME the appearance of dimmings, the onset of the EIT wave, and the flare peak occurred at almost the same time (i.e., within the 17 minute cadence of the EIT observations for this event). In a detailed comparison of a prominence eruption and EIT coronal dimmings, Gopalswamy & Hanaoka (1998) showed that the dimmings started much earlier than the prominence eruption. Unfortunately, at present, the cadence of solar full-disk, space-based data, such as EIT images, is limited by telemetry, and it is not always possible to determine the exact chronology of events (Thompson et al. 2000), while the high-cadence *TRACE* data (Handy et al. 1999) have a limited field of view and do not provide a global view of eruptive events.

Transient coronal holes have been traditionally observed from space, but they can also be observed from the ground in the He I 1083 nm line (Harvey & Recely 1984; Harvey et al. 1996). Wave transients associated with CMEs have also been detected in He I 1083 nm observations (Vršnak et al. 2002; Gilbert et al. 2004). The He I 1083 nm line is formed in the upper chromosphere and lower transition region, but it is strongly affected by the overlying coronal radiation at $\lambda < 50.4$ nm penetrating into the upper chromosphere. In He I 1083 nm images, areas underlying regions of high coronal emission are usually darker, while areas underneath regions of low coronal emission, such as coronal holes, are brighter. For this reason, transient coronal holes appear as brightening regions in He I 1083 nm that are cospatial and form at about the same time as EUV dimmings. The contrast of transient coronal holes in He I 1083 nm is lower than for EUV observations, such as those made by EIT, which makes the temporary holes more difficult to identify, and a smaller number of transient coronal holes is detectable in He I 1083 nm than in the EUV and X-ray. The advantage of the He I 1083 nm observations made at the Mauna Loa Solar Observatory (MLSO) is their high temporal cadence that allows us to study the appearance and evolution of transient coronal holes and other transient phenomena more accurately than with space data alone. In addition, transient coronal holes, when observed in He I 1083 nm, are not affected by the presence of bright coronal structures intercepting the line of sight, as they are in EUV and X-ray observations away from disk center. The He I 1083 nm line is optically thin (Jones 1994), but it is formed in a very narrow region, when compared with the coronal scale height. Hence, He I 1083 nm observations should give us precise information on the morphology of the holes at any location on the solar disk.

In this study we searched for cases in which transient coronal holes developed in association with a CME and were visible in both EUV data from space and in the ground-based MLSO observations in the He I 1083 nm line. We found that, when the IR He I 1083 nm brightenings are visible, they form at about the same time as the EUV Fe XII 19.5 nm dimmings, and there is good spatial correlation between the brightening regions in He I 1083 nm and the EUV dimmings. The motivation for this research is to better understand the physical processes taking place in the source regions at the time of a CME onset. For this purpose, we investigated the relationship between the formation of transient coronal holes and the other manifestations of a CME. In this paper we examine six events, listed in Table 1, and present two of these events in detail to demonstrate the capability of He I 1083 nm observations to detect the solar disk signatures of CMEs. In § 2 we briefly describe the instruments and data used in our research. In § 3 we discuss the importance of chromospheric observations in studies of transient coronal holes. In § 4 we present the analysis of two eruptive events with associated transient coronal holes on 2001 January 20 (Figs. 1–6) and 2000 November 25 (Figs. 7–10). Finally, in § 5 we summarize our findings and discuss the properties of transient coronal holes.

2. INSTRUMENT DESCRIPTIONS

For this study we used primarily EUV observations obtained with the EIT instrument (Delaboudinière et al. 1995) on *SOHO* and He I 1083 nm observations from the Chromospheric Helium I Imaging Photometer (CHIP) at MLSO. We also used Hα data from the Polarimeter for Inner Coronal Studies (PICS) at MLSO, which are taken simultaneously with the CHIP He I observations and are thus very useful to study the evolution of flare events associated with the transient coronal holes. Finally, we used data from the *SOHO* LASCO (Brueckner et al. 1995) and MLSO Mk4 coronagraphs to identify the CMEs associated with the events studied and to compute the CME trajectories.

2.1. *SOHO EIT*

The EIT instrument provides full-disk (1024×1024) images of the solar inner corona and transition region in the EUV. EIT observes the Sun in four wavelength regions centered at 17.1, 19.5, 28.4, and 30.4 nm (Delaboudinière et al. 1995; Moses

et al. 1997; Dere et al. 2000). During normal operations, images are acquired approximately every 12 minutes with the 19.5 nm filter and 4 times a day with all four filters. The 19.5 nm bandpass is chosen as the preferred filter for the high contrast and high sensitivity to quiet-Sun structures. The temperature response of the 19.5 nm filter peaks at about 1.5×10^6 K and is dominated by the Fe XII emission lines at 19.2, 19.4, and 19.5 nm, the latter being the strongest. During flare events there can be significant contribution from the Fe XXIV line at 19.2 nm (W. M. Neupert 2001, private communication). For simplicity, in this paper we refer to the 19.5 nm bandpass as the Fe XII 19.5 nm line.

2.2. *MLSO PICS, CHIP, and Mk4*

The PICS, CHIP, and Mk4 instruments are located at MLSO, which operates daily, weather permitting, collecting data beginning at about 1700 UT. Before 2003 January, data were taken for approximately 5 hr per day. Since 2003 January, the observing day has been extended to 9 hr. The three instruments normally acquire images with a 3 minute temporal cadence, but thanks to a recent upgrade of the MLSO computing system, it is now possible to run the instruments at a higher cadence, up to one image per minute, during special observing campaigns.

The PICS instrument is a telescope with a removable occulting disk used to make observations of the limb or disk in the Hα line at 656.3 nm. The disk and limb images are acquired using a narrowband filter of ± 0.05 nm and a broadband filter of ± 1.0 nm, respectively. The bandwidth of the PICS disk instrument allows for line-of-sight velocities of the order of 40–45 km s^{-1} before an erupting filament on the disk is Doppler shifted out of the filter. However, the relatively cool prominence material can be heated and ionized during an eruption and, as a consequence, progressively fade in the Hα line. For this reason, disappearing filaments in Hα images can provide useful information about filament eruptions, but velocity data, such as the ones provided by the CHIP instrument, are necessary to determine the dynamics of filament eruptions.

The CHIP instrument (Elmore et al. 1998; MacQueen et al. 1998) provides full-disk and off-limb He I 1083 nm intensity and velocity images. The He I 1083 nm line, which is seen in absorption on the solar disk, is dominated by the underlying photospheric continuum. To enhance the contrast of chromospheric structures, the helium intensity is often measured relative to the nearby continuum. In the original CHIP observing configuration, the tunable Lyot filter ($\approx$0.13 nm bandpass) was sequentially positioned at three wavelengths: in the center of the He I line at 1083.03 nm, and to ± 0.15 nm. Since 2000 February, CHIP data have been acquired using seven filter positions covering the spectral region from $\approx$1082.6 to 1083.4 nm. The seven-filter configuration gives a better determination of the helium intensity and velocity and allows the instrument to follow more accurately the dynamics of filament eruptions. If a filament has a line-of-sight velocity of over $\approx$40 km s^{-1}, it will not be visible in the filter centered to the He I line, but it will be seen in the blue or red filters, depending on whether the velocity is directed toward or away from the observer. The line-of-sight velocities of an erupting filament can be over 100 km s^{-1} before a filament is Doppler shifted outside of the outer CHIP filters. Combining the signal in the seven filters allows us to determine the direction and line-of-sight velocity.

3. OBSERVATIONS OF THE SOLAR CHROMOSPHERE

Observations in the He I triplet at 1083 nm and in the Balmer Hα line at 656.3 nm are normally used to monitor the solar chromosphere, since both lines form in the upper chromosphere and can be observed from the ground. Their heights of formations are different in different solar structures, but typical values for Hα range from 1500 (above sunspots) to about 2700 km (White & Wilson 1966). The He I lines are formed in a relatively thin shell of a few hundred kilometers. The helium height of formation has been deduced by limb measurements in the He D3 lines (White 1964; Zirin 1975) and, more recently, in the He I 1083 nm line itself (Schmidt et al. 1994; Penn & Jones 1996). Typical values range between 1500 and 2400 km, in fairly good agreement with values derived from radiative transfer computations based on semiempirical models of the chromosphere and transition region (Fontenla et al. 1993).

Simultaneous images taken in the He I 1083 nm and Hα lines have shown that there is good agreement in position and shape of both bright and dark Hα features with He I 1083 nm enhanced absorption: active regions, filaments, and two-ribbon flares in the Hα image all appear as dark features in the He I 1083 nm image. However, the relationship between the two line intensities is not simple (Giovanelli et al. 1972), and when solar images are recorded at moderately high resolution, such as in the MLSO observations, differences in the fine structure of these solar features become apparent. These differences are not surprising because the excitation mechanisms for these two chromospheric lines are very different.

Hα observations are made at several observatories and have been traditionally used to study filaments and the solar chromosphere in general. They provide accurate information on the site and growth of flares and have also been used to detect waves. He I 1083 nm observations are currently made at the National Solar Observatory (NSO) at Kitt Peak and MLSO. The properties of the He I 1083 nm line are described below.

3.1. He I 1083 nm *Observations*

The IR He I 1083 nm triplet consists of the lines at 1083.034, 1083.025, and 1082.908 nm, with the first two lines blended together and 8 times stronger than the third. The lines correspond to the transition $1s2s\ ^3S–1s2p\ ^3P$ of the ortho-helium, where the $2s$ state acts as a ground state. The He I 1083 nm line is seen in absorption on the solar disk, except in flare kernels, where it can go into emission (Penn & Kuhn 1995), and it is seen in emission above the solar limb. Solar disk observations show that the line absorption profile changes significantly in different solar structures: absorption is stronger in plages and filaments than in the quiet Sun, and it is also enhanced at the chromospheric network boundaries, while it is weak in coronal holes (Harvey & Livingston 1994; Jones 1994).

The formation of the He I multiplet at 1083 nm is quite complex. The He I 1083 nm excitation of the line is driven by the photospheric radiation, but the population of the He I 1083 nm triplet states is strongly influenced by coronal radiation at wavelengths shortward of 50.4 nm (i.e., with energy greater than 24.6 eV ionization potential of the para-helium). This coronal radiation penetrates into the chromosphere where the lower level of the He I 1083 nm line is populated via photoionization of the He I 1083 nm singlet ground state followed by recombination to the triplets levels (Zirin 1975, 1988). If photoionization recombination were the only formation mechanism of the He I 1083 nm line, the observed absorption would not depend on the local temperature. However, collisional excitation of helium by electrons at temperature greater than 20,000 K can also play a role in the formation of the He I 1083 nm line, especially in the lower transition region (Andretta & Jones 1997). The amount of absorption in He I 1083 nm depends on the incident coronal illumination

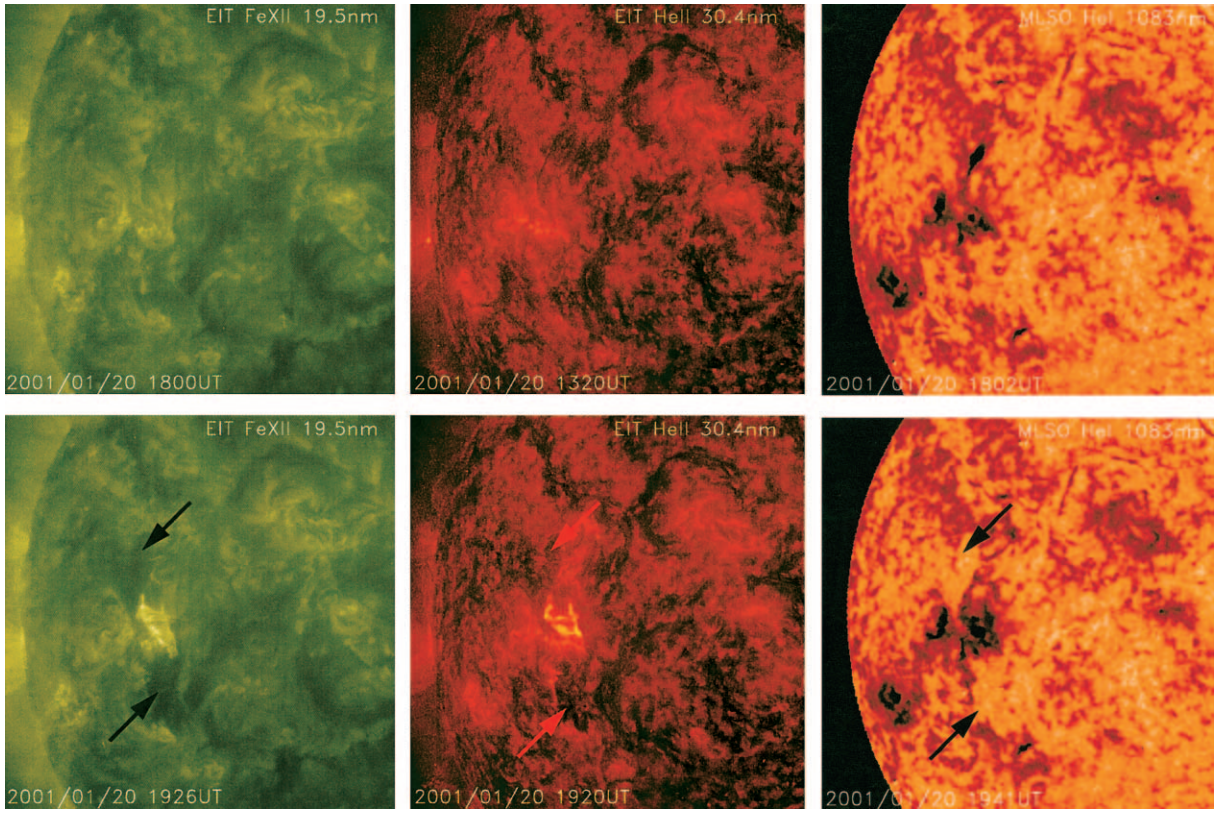

FIG. 1.—Formation of transient coronal holes on 2001 January 20 as observed by *SOHO*/EIT in the EUV Fe XII 19.5 nm and He II 30.4 nm lines and by the MLSO/CHIP instrument in the IR He I 1083 nm line. Images in the low corona and chromosphere are shown before (*top panels*) and after (*bottom panels*) the eruption, when transient coronal holes had already reached full development. Transient coronal holes, indicated by arrows, appear as dimming regions at EUV wavelengths and as brightening regions of reduced network contrast in the He I 1083 nm line. Note that the location and shape of the transient coronal holes is alike in all the lines.

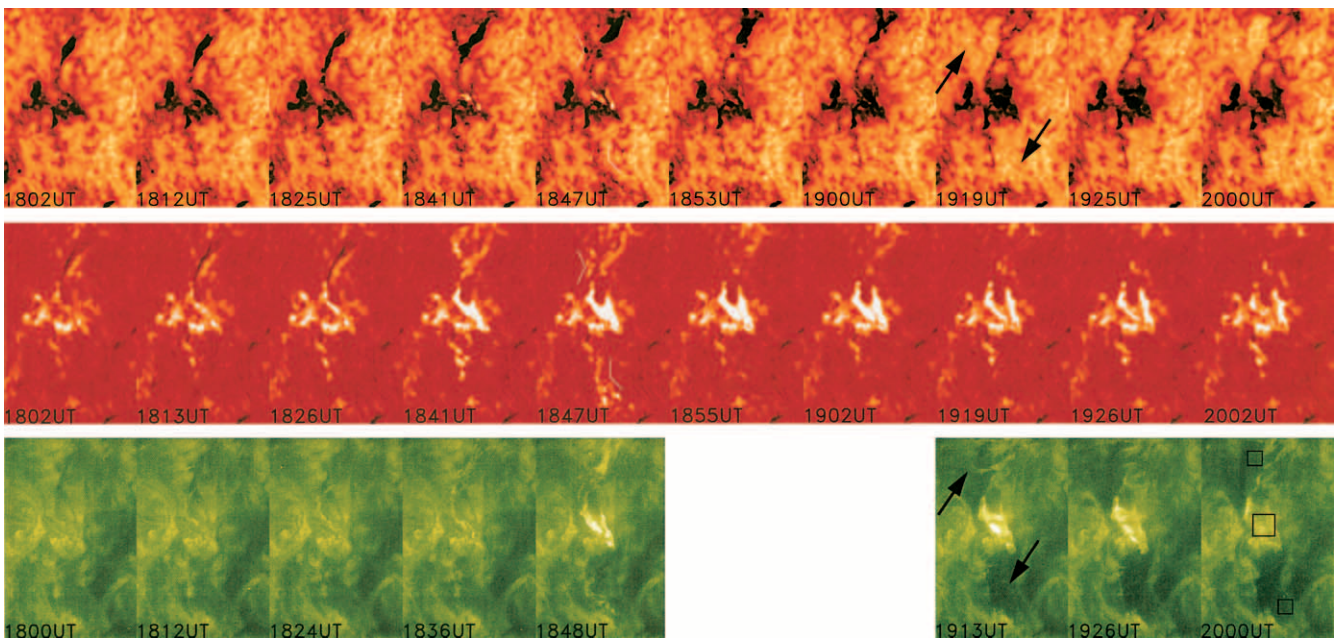

FIG. 2.—Sequence of images centered on AR 9313 on 2001 January 20 shows the evolution of the chromosphere and corona during and after the eruption of the filament, the two-ribbon flare, and the formation of the transient coronal holes. He I 1083 nm images (*top*) are from MLSO/CHIP, Hα 656.3 nm images (*middle*) from MLSO/PICS, and Fe XII 19.5 nm images (*bottom*) from *SOHO*/EIT. The He I 1083 nm and Hα images are taken within a minute. The images in Fe XII 19.5 nm line are close in time but not simultaneous. We note that the kernels of the two-ribbon flare go into emission, i.e., appear bright, in the He I 1083 nm at 1841–1853 UT. At 1847 UT, secondary flaring is seen as short-lived dark features in He I 1083 nm that correspond to bright features in Hα and are indicated in white. The location of the transient coronal holes is indicated by black arrows, while the boxes in the EIT image at 2000 UT identify the regions used for the light curves in Figs. 4 and 5.

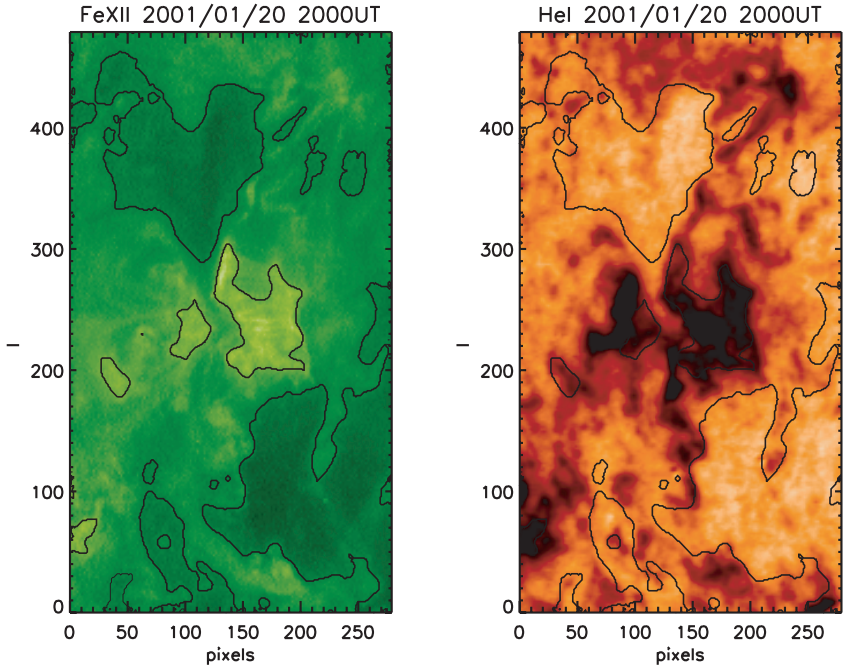

FIG. 3.—Images of the fully formed transient coronal holes on 2001 January 20 in He I 1083 nm (*right*) and Fe XII 19.5 nm (*left*). The equal intensity contours for dark and bright features in the Fe XII 19.5 nm line are overplotted to both images to show the good spatial correspondence of the flare and transient coronal holes, at the two wavelengths. The transient coronal holes are located above and below the flaring active region. (Images have been aligned and the helium image has been resized to the EIT image. The spatial scale is of 2″.62 per pixel.)

and on the density of the transition region (for a more complete discussion of the neutral helium lines see Fontenla et al. 1993; Avrett et al. 1994; Andretta & Jones 1997 and references therein).

Because the intensity of the He I 1083 nm line is largely modulated by the overlying coronal radiation, especially in regions of relatively weak magnetic fields, images in this line differ from images in other chromospheric lines, such as Hα. The most significant difference is that coronal holes, being regions of reduced coronal emission, appear as relatively bright regions in He I 1083 nm, indicating weaker helium absorption. For this reason, He I 1083 nm observations have been used since the 1970s to infer the boundaries of coronal holes, when coronal observations were not available (Harvey & Sheeley 1979). It has also been known for a long time (McCabe & Mickey 1981) that regions of reduced absorption can be seen in He I 1083 nm adjacent to or along filaments as relatively bright "helium lanes." These observations were interpreted as an indication that filament channels correspond to relatively low density regions in the corona. It is thus not surprising that transient coronal holes can also be detected in the He I 1083 nm line.

Studies of transient coronal holes using the He I 1083 nm line were very limited in the past (Harvey & Recely 1984; Harvey et al. 1996) because of the scarcity of high-cadence observations in this line or in other helium lines. A comparison of coronal holes as seen in He I 1083 nm with the evolution of large-scale, bright arcades in X-ray at the times of filament eruptions has been made by Harvey et al. (1996) using NSO/Kitt Peak He I 1083 nm and *Yohkoh* SXT images. They noted the expansion of existing coronal holes located next to the erupting filament and the appearance of new, transient coronal holes and interpreted these observations as a temporary opening of previously closed magnetic fields. NSO/Kitt Peak normally acquired only one image per day in the He I 1083 nm line. This was insufficient to study the evolution of transient coronal holes. The CHIP instrument at MLSO records He I 1083 nm images with a 3 minute temporal cadence. This higher cadence of the observations is appropriate to study the appearance and evolution of transient coronal holes. Instruments on the SOLIS program, which started in late 2003 at NSO/Kitt Peak, will acquire He I 1083 nm full-disk images with 1 minute cadence, providing another opportunity to study transient coronal holes (J. Harvey 2004, private communication).

4. ANALYSIS OF CME EVENTS ASSOCIATED WITH TRANSIENT CORONAL HOLES

We examined six cases, summarized in Table 1, when transient coronal holes were detected both in the EUV by the EIT telescope and in the IR He I 1083 nm line by the CHIP instrument at MLSO. We studied the formation of the transient coronal holes, compared their characteristics at different wavelengths, and studied their relationship with the flare, filament eruption, and CME. To demonstrate the usefulness of the He I 1083 nm observations in the study of CME onsets, we present a detailed description of two of the cases studied below. We show one example of transient coronal holes associated with a filament eruption on 2001 January 20 where the EUV dimmings and the He I 1083 nm brightenings are located next to the flaring region on opposite sides of the polarity inversion line (Figs. 1–3). While this is a common morphology, many transient coronal holes do not have this symmetry and there are instances when only one hole is clearly visible, as in our second example on 2000 November 25 (Figs. 7 and 8). Transient coronal holes are not easy to identify in the He I 1083 nm images because of the low contrast of coronal holes in this line. Subtraction of a reference, pre-event image can help to enhance the contrast of the regions where the transient coronal holes form, but difference images can also be confusing since bright regions may be the result of an increased brightening (as in a transient coronal hole) or of the disappearance and attenuation of a dark feature (as in

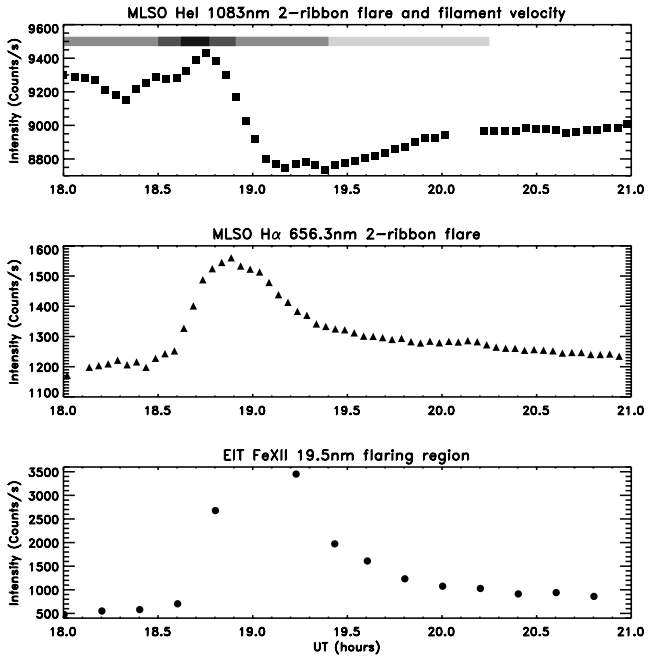

FIG. 4.—Evolution of the flare on 2001 January 20 for the He I 1083 nm, Hα, and Fe XII 19.5 nm lines. The light curves have been computed for the region centered on the flare identified in Fig. 2. Images have been carefully aligned and corrected for differential rotation, to ensure that we tracked the same region on the Sun from image to image. The Hα flare reached the maximum intensity and area at 1853 and 1850 UT, respectively. The relative brightening in He I 1083 nm during the early phase of the flare corresponds to the time when bright flare kernels were visible. The top bar shows the time when outward filament velocity was detected by the He I 1083 nm instrument, with the darker colors indicating higher velocities. The erupting filament reached its maximum velocity during the rising phase of the flare. (Data are corrected for instrumental effects and normalized to the exposure time. He I 1083 nm, Hα images are corrected for center-to-limb variations.)

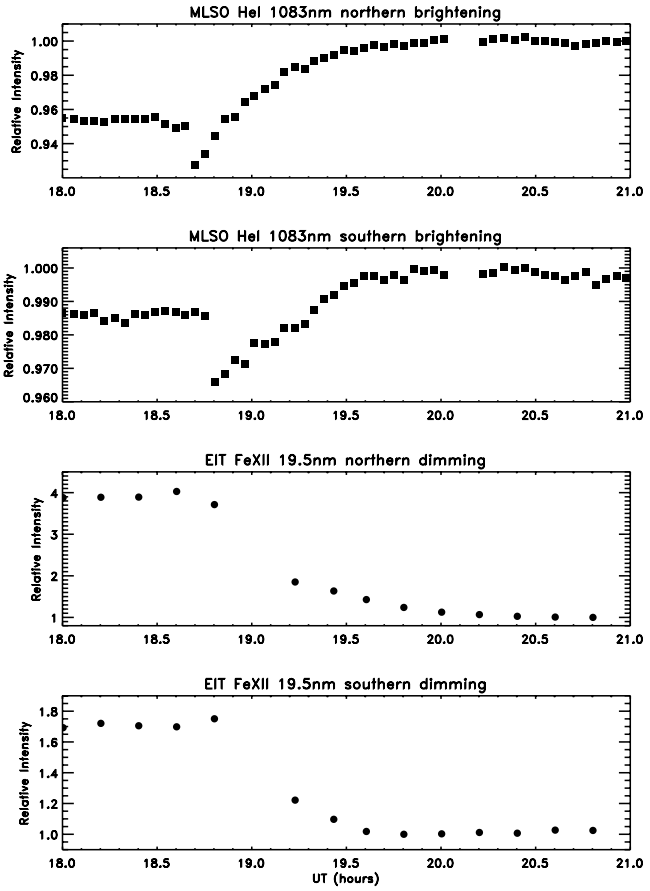

FIG. 5.—Evolution of the northern and southern transient coronal holes on 2001 January 20 for the He I 1083 nm and Fe XII 19.5 nm lines. The light curves have been computed for the two regions identified in Fig. 2. Note the temporary darkening in the He I 1083 nm light curves that precedes the brightening and corresponds to short-lived flaring occurring within the region where the transient coronal holes form. (Data are given in relative intensity units: He I 1083 nm and Fe XII 19.5 nm are normalized to the maximum and minimum value, respectively.)

a filament eruption). In the examples below, we use both direct and subtraction images, but we rely on light curves and intensity scans (Figs. 5, 6, and 10) to give a quantitative description of the transient coronal holes formation and evolution.

4.1. *2001 January 20 Event*

This event occurred on the east side of the Sun, in active region AR 9313 and was associated with a filament eruption and a fast CME. The chronology of this event is illustrated by the images and light curves in Figures 1–6. The filament was located at an average latitude and central meridian longitude of N02, E41, the flare was centered at S06, E39.

MLSO/CHIP He I data indicate the filament was already active (i.e., showed outward motion) at the beginning of the MLSO observing day at 1756 UT. The filament line-of-sight velocity systematically increased starting at 1831 UT, reaching its maximum at 1837–1846 UT. By 1850 UT the filament disappeared in Hα, but it remained visible longer in He I 1083 nm. This is because the set up of the MLSO/CHIP instrument allows for larger velocities before the filament is Doppler shifted out of its bandpass. Velocity stayed at high values until 1855 UT, then decreased and after 2015 UT no significant velocity signal was detected. Some downward motion was detected in the red helium filters during the course of the eruption, especially in its late phase at 1849–1911 UT, indicating that part of the filament material did not erupt and drained back toward the solar surface, which is a common feature of prominence eruptions.

The temporal evolution of the flare is shown by the series of images in Figure 2 and by the light curves in Figure 4. In the Hα line, the impulsive phase of the two-ribbon flare began at 1837 UT, the flare peaked at 1853 UT and then slowly faded. This is consistent with the GOES X-ray flare which started at 1833 UT and peaked at 1850 UT. In He I 1083 nm, the two-ribbon flare appeared as two dark features of increased absorption at about the same location of the Hα ribbons. In the early phase of the flare, from 1838 to 1856 UT, bright flare kernels were visible (see Fig. 2), as the center of the He I 1083 nm line went into emission; this is often seen in the MLSO He I 1083 nm data during intense flares. The sequence of the Fe XII 19.5 nm images was limited by the lower cadence of EIT and by the data gaps due to observations taken with the other EUV filters, so we cannot establish the flare peak time. We note that the flaring region in Fe XII 19.5 nm was brighter at 1913 UT than at 1848 UT, in contrast with the Hα observations. This is because bright flare loops were visible at 1913 UT in Fe XII 19.5 nm, while the Hα flare footpoints had already started to decay in intensity. Hα flare loops are clearly seen above the solar limb in MLSO images but are typically not detectable against the disk.

The formation of the transient coronal holes is shown by the images in Figures 1 and 2, and by the light curves in Figure 5. Dimming regions in the Fe XII 19.5 nm were first visible at the same time of the two-ribbon flare in the 1848 UT image. They

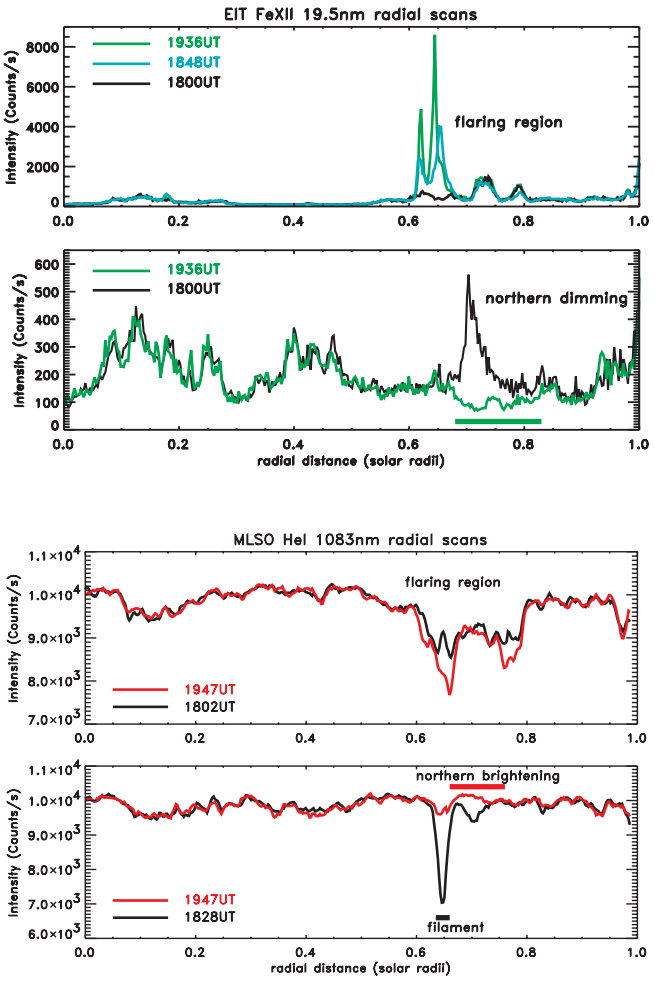

FIG. 6.—Radial scans before and after the eruption of 2001 January 20. They show the variation in relative intensity at the location of the flare and of the northern transient coronal hole at the solar position angle $\theta = 95^\circ$ and 78°, respectively. Flare loops are bright in the Fe XII 19.5 nm line, while the two-ribbon flare is dark in He I 1083 nm line. Transient coronal holes correspond to a decrease in EUV emission and to a reduced absorption in He I 1083 nm.

rapidly increased and darkened and by 1913 UT were fully developed. At about the same time, two regions of increased brightness, cospatial to the EUV dimmings, became visible, in He I 1083 nm. The two transient coronal holes were not completely symmetric in shape: the southern one had a more diffuse appearance and covered a larger area than the one in the north (Figs. 2 and 3). In He I 1083 nm transient coronal holes appear as relatively bright regions. Within these regions a considerable attenuation of the chromospheric network pattern is noticeable as the holes form at 1847–1925 UT, as illustrated in Figure 2. Two thin, dark lanes, indicated in white in Figure 2, are also visible at about 1847–1850 UT in He I 1083 nm images in the regions where the transient coronal holes will form. These darkenings are very short lived (i.e., minutes) and correspond to relatively bright features in the simultaneous Hα images. It is difficult to identify them in the Fe XII 19.5 nm images because of the EIT cadence, but the image at 1848 UT suggests they appear as brightenings at EUV wavelengths. These rapid intensity changes are likely caused by flaring, since they are not associated with a significant velocity signal. They are responsible for the decreased intensity seen around 1850 UT in the He I 1083 nm light curves preceding the increase associated with the formation of the transient coronal holes (Fig. 5).

In Figure 6 we show radial scans crossing the active region and the northern coronal hole for the Fe XII 19.5 nm and He I 1083 nm observations to illustrate the brightness changes in these regions at both wavelengths. Note the increased helium absorption at the site of the two-ribbon flare and the reduced helium absorption at the location of the transient coronal hole in the He I 1083 nm data. Intensity values within the transient coronal holes are $\approx$10,100–10,200 counts s^{-1} for He I 1083 nm and 50–60 counts s^{-1} for Fe XII 19.5 nm. These are comparable to intensity values found within nontransient coronal holes. We note that the relative intensity change in He I 1083 nm is only a few percent compared to a factor of 2 or more in Fe XII 19.5 nm. The average photospheric magnetic flux within the region where the holes form, as determined by the NSO/Kitt Peak magnetogram for that day, is found to be about 11.5 Mx cm^{-2}, similar to values found within other coronal holes.

There was a wave occurring almost simultaneous to the flare onset, with two noncircular fronts moving north and south of the active region. The start time of the wave has been estimated at 1837 UT (Gilbert & Holzer 2004); thus it preceded the transient coronal holes formation. A second wave followed at 1843 UT, about the same time the transient coronal holes appear. The wave transient was noticeable in both Fe XII 19.5 nm and He I 1083 nm images, but was not obvious in Hα. Brightenings and filament motions were noticeable in Hα images, shortly after the eruption, in two active regions located at N05, E08 and N04, W17. The brightenings occurred at 1952–1955 and 2013–2016 UT, respectively, and were also detectable in He I 1083 nm images as darkenings, but we could not establish with confidence if such activity was caused by the passage of the wave front since the wave was not visible at these locations.

This event was associated with a wide CME observed by the MLSO/Mk4 and *SOHO*/LASCO. The CME was first detected by Mk4 at an apparent height of $\approx$1.5 solar radii at 1850 UT and became visible in the LASCO/C2 field of view at 1931 UT. The leading front of the CME moved in the LASCO field of view with no significant acceleration and a projected velocity of over 800 km s^{-1}. This velocity is a lower estimate, because the source region is far from the solar limb, thus we expect the CME not to be in the plane of the sky. Assuming that the CME was centered on the flare site and moved radially outward, the velocity would have been over 1000 km s^{-1}. Combining the low corona Mk4 data with the LASCO data gave an estimated start time of the CME at 1830–1840 UT, but the acceleration phase was not well covered by our observations since it occurred in part below the Mk4 field of view and the CME may have started earlier.

4.2. *2000 November 25 Event*

This event occurred within AR 9236, located at an average latitude and central meridian longitude of N20, W25. The active region had recently developed a beta-gamma configuration and had been very active for the previous 24 hr, producing a series of powerful CMEs that caused significant geomagnetic activity during the period November 27–29.

The event started with a fast filament eruption within the active region beginning at about 1715 UT. The erupting filament material was clearly seen in the MLSO Hα and He I 1083 nm images and had a line-of-sight velocity of above 80 km s^{-1}. A two-ribbon flare was detected in both wavelength starting at about 1714 UT within AR 9236. Another, brighter flare within the same active region shortly followed at 1837–1840 UT. A

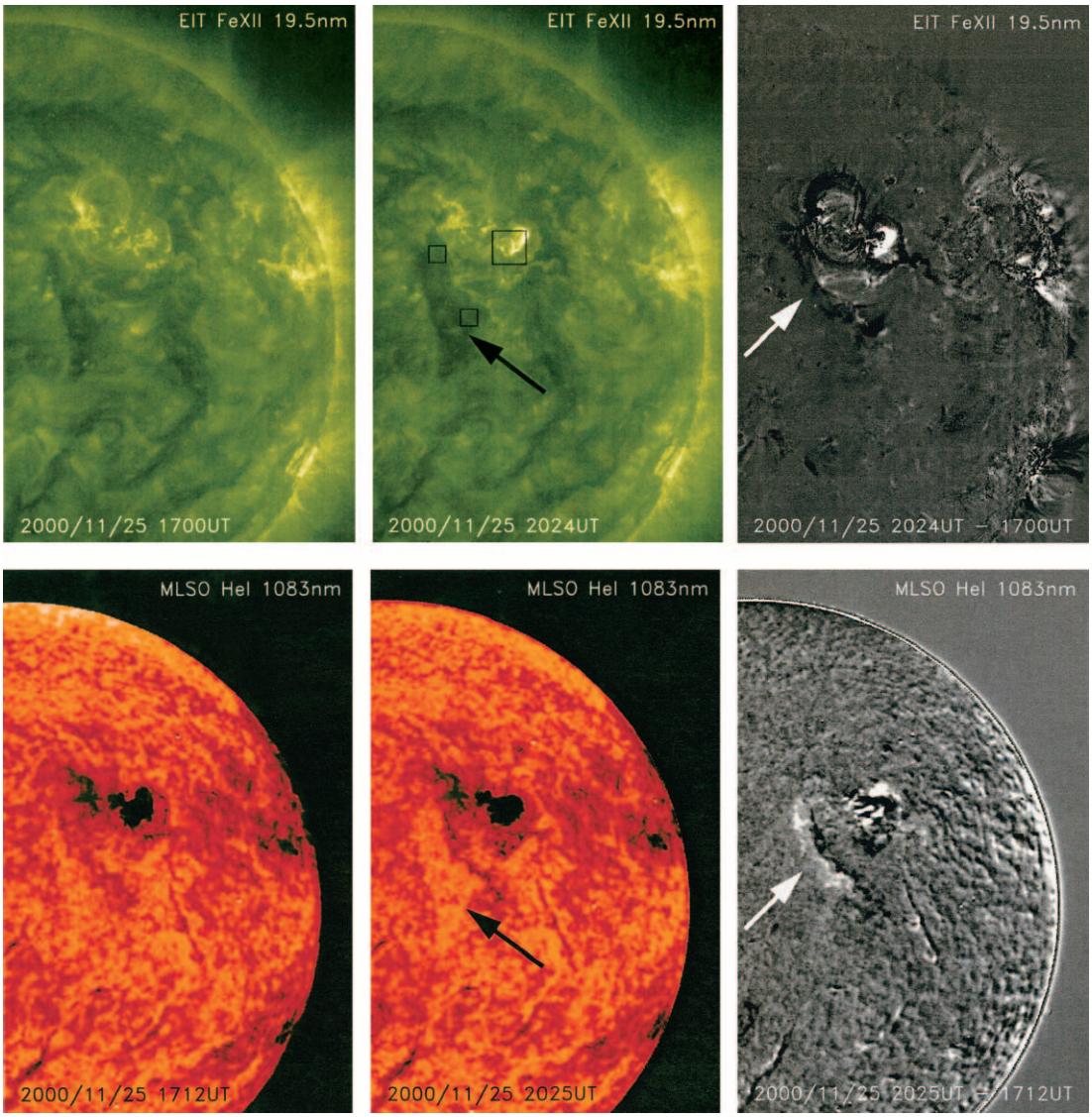

FIG. 7.—Evolution of a coronal hole in response to a CME eruption as seen in Fe XII 19.5 nm (*top*) and in He I 1083 nm (*bottom*) on 2000 November 25. The left and center images were made before and after the eruption, respectively. We used the same color scale for both the preevent and the postevent images to demonstrate the increase in size and contrast of the coronal hole, indicated by the black arrow. The images on the right are difference images, they have been computed after rotating the preevent image to the time of event image. The enlargement of the preexisting coronal holes is seen as a brightening in He I 1083 nm and as a darkening in Fe XII 19.5 nm indicated by the white arrow. The boxes in the center top panel indicate the regions used to compute light curves in Figs. 9 and 10.

small velocity signal was detected beginning at 1838 UT, indicating that a second piece of filament erupted.

Two CMEs with projected velocity of over 600 km s^{-1} were associated with this activity. These velocities are largely underestimated, since the source region of the CME was at almost 60° from the solar limb. The second CME was detected by the Mk4 instrument, but we cannot determine the start time of this CME with confidence because of the large projection effect. It likely started before 1830 UT. A transient coronal hole near the flare site started at about 1843 UT, several minutes after the second flare and CME. A wave disturbance was detected in the Fe XII 19.5 nm and He I 1083 nm that consisted of more than one wave front (Gilbert & Holzer 2004), originating at the active region site, from 1820 to 1843 UT. The last wave front began at the same time of the transient coronal hole.

The temporal evolution of the second flare in He I 1083 nm and Fe XII 19.5 nm is shown by the light curves in Figure 9. A gap in the Hα observation at MLSO did not allow us to follow the evolution of the second flare in this line. The start and peak of the *GOES* X-ray flare were at 1833 UT and 1844 UT, respectively. The He I 1083 nm showed bright flare kernels starting at 1837 UT. Another flaring region, outside of the active region, was visible at the edge of the transient coronal hole as a dark rim in He I 1083 nm and a bright rim in Fe XII 19.5 nm (see Fig. 7). In Fe XII 19.5 nm bright arcades, whose footpoints started near the active region and ended at this bright rim, became visible at 2112 UT.

In this event, we did not see the appearance of two, symmetric transient coronal holes, but instead the enlargement of a preexisting coronal hole, situated next to the active region, on the southeast side. The hole was already well formed at the time of the event, and had darkened in Fe XII 19.5 nm during previous eruptions of the same active region. To illustrate the change in the preexisting coronal hole region, we show images before and two hours after the eruption, as well as their differences, in Figure 7. These observations show that the coronal hole after the CME had significantly extended in size and the intensity contrast had increased. In the difference images, the enlargement of the hole appears as a darkening in Fe XII 19.5 nm and as a brightening in He I 1083 nm. To illustrate the good spatial

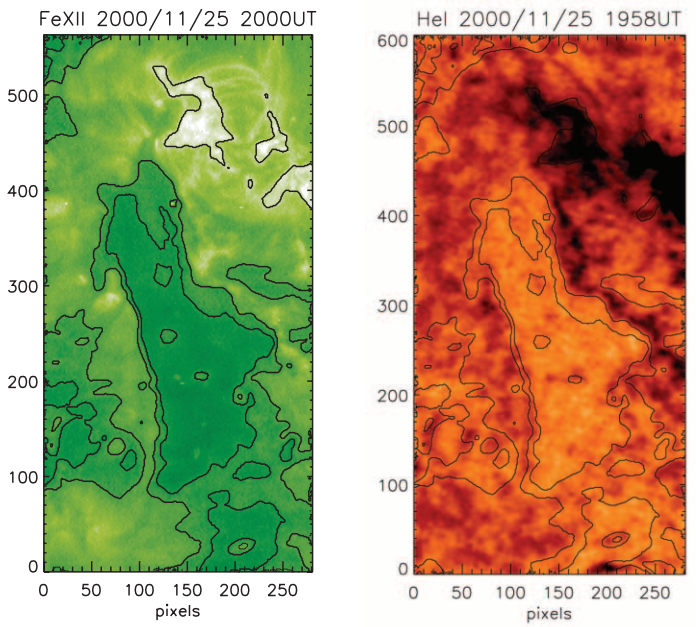

FIG. 8.—Images of the fully formed transient coronal hole on 2000 November 25 in He I 1083 nm (*right*) and Fe XII 19.5 nm (*left*). The equal intensity contours of dark and bright features based on the Fe XII 19.5 nm line are overplotted to both images to show the good spatial correspondence of the transient coronal hole in the two lines. (Images have been aligned and the helium image has been resized to the EIT image. The spatial scale is of 2.″62 per pixel.)

correspondence between the transient coronal hole as it appeared in the Fe XII 19.5 nm and He I 1083 nm lines, we show in Figure 8 an enlargement of the fully formed transient coronal hole. We overplot constant intensity contours in the Fe XII 19.5 nm line to both images to better compare the shape of the hole at the two wavelengths. The transient coronal hole formation is shown by the light curves in Figure 10 for two subregions within the hole. The brief darkening in He I 1083 nm and brightening in Fe XII 19.5 nm at about 1840–1848 UT, are associated with short-lived flaring and the wave front crossing the region where the transient coronal hole formed. Relative intensity values within the holes are 50 counts s^{-1} or less for Fe XII 19.5 nm and over 10,050 counts s^{-1} for He I 1083 nm, while the average photospheric magnetic flux is estimated about 5.8 Mx cm^{-2}.

5. DISCUSSION AND CONCLUSIONS

Despite the extensive research on CMEs, the origin and early development of CMEs are still not well understood. To gain a

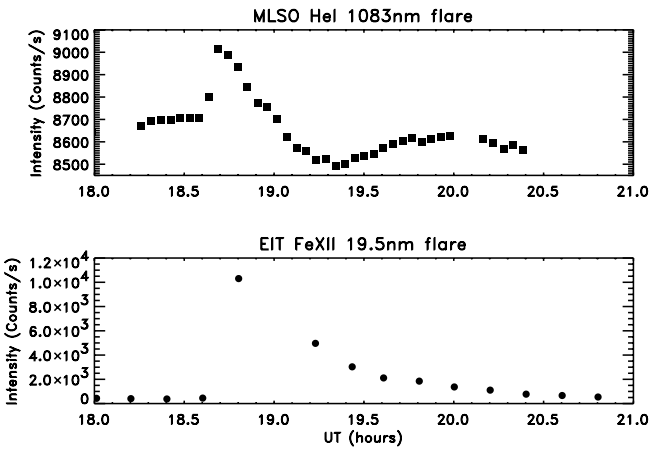

FIG. 9.—Evolution of the flare starting at about 1835 UT on 2000 November 25 in the He I 1083 nm and Fe XII 19.5 nm lines. The light curves have been computed for the region identified in Fig. 7. The increase in He I 1083 nm relative intensity during the early phase of the flare is due to the bright flare kernels.

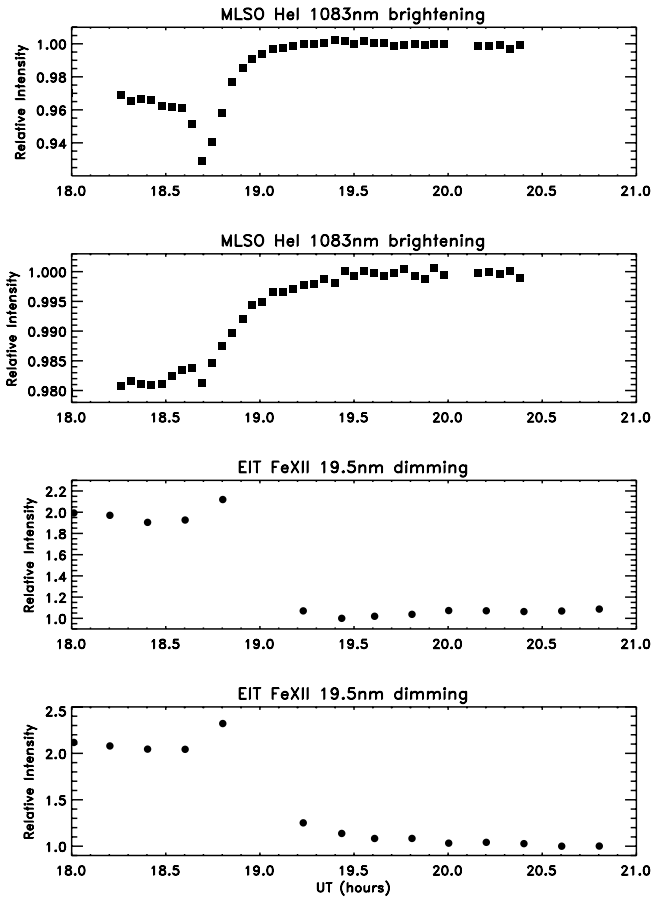

FIG. 10.—Evolution of the transient coronal hole on 2000 November 25 as observed in the He I 1083 nm and Fe XII 19.5 nm lines. The light curves have been computed for the two regions identified in Fig. 7. The upper region corresponds to the top curve and the lower region to the bottom one. (Data are given in relative intensity units: He I 1083 nm and Fe XII 19.5 nm are normalized to the maximum and minimum value, respectively.)

better understanding of CMEs and their causes, it is important to accurately determine the sequence of events occurring in the process of such eruptions. This involves looking at the disk manifestations of activity in the low corona and chromosphere associated with CMEs. Combination of EUV and X-ray observations from space with high-cadence ground-based observations provide a means to accurately establish the start time and evolution of these events.

We studied the formation of transient coronal holes associated with CMEs and their relationship with other CME manifestations on the solar disk, such as filament eruptions, waves, and flares for six cases summarized in Table 1. In addition to space data, we have used high-cadence, full-disk observations from MLSO. In § 4 we presented an observational description of two cases where CME associated, transient coronal holes on the solar disk were visible at both EUV and He I 1083 nm wavelengths.

For the cases studied, we find that the appearance of transient coronal holes at the EUV wavelengths observed by EIT and in the IR He I 1083 nm line occurs at the same time, within the 12 minute cadence of the EIT observations. Comparison of almost simultaneous images shows good correspondence in the shape and location of transient coronal holes in the Fe XII 19.5 nm and He I 1083 nm lines as illustrated in Figures 3 and 8. This indicates that the He I 1083 nm appearance of transient coronal holes as brightening regions is likely caused by the change in the above coronal radiation penetrating into the chromosphere. Typical boundaries of coronal holes in the MLSO images are over 10,000 km wide. Thus, their size is consistent with the hypothesis that the He I 1083 nm line is dominated by the photoionization and recombination mechanism (Gilbert et al. 2004). In this mechanism, the He I 1083 nm bright regions associated with transient coronal holes, or longer lived coronal holes, are caused by the decrease in the coronal EUV emission below 50.4 nm in the overlying coronal holes. However, there is at least one case, not discussed here, on 1998 December 18 (T. Forbes 2004, private communication) where Fe XII 19.5 nm dimmings have similar shape and location to the He I 1083 nm brightenings but are somewhat larger. In this case, the transient coronal holes form very close to the flare site, so it is possible that the intense coronal radiation from the flaring region excite the He I 1083 nm line beneath the dimming region in the areas closer to the flare, producing a smaller brightening region.

The sensitivity of the He I 1083 nm line to density changes in the corona is not as high as in EUV and X-ray observations as illustrated by Figures 5 and 10. This can explain why there are several cases when EUV dimmings are not associated with obvious He I 1083 nm brightenings. We speculate that they may occur in regions of already low He I 1083 nm intensity and/or where the relative change in EUV emission within the dimming regions is low. A study of events when EUV dimmings do not correspond to He I 1083 nm brightenings is necessary to fully understand the differences between these lines and it is a subject for future research. It is worth noting that there are also several CMEs that show no detectable decrease in EUV emission (Thompson et al. 2000).

The formation of transient coronal holes, for the events studied, occurs during the impulsive phase of the flare as observed in EUV and Hα; usually when, or immediately after, bright flare kernels are seen in He I 1083 nm. The estimated start time of coronal waves and the appearance of the transient coronal holes is found to be almost simultaneous for at least two cases, but more events are necessary to investigate their relationship. For the cases examined, we find that when transient coronal holes are seen in He I 1083 nm, they are accompanied by a CME. The time of appearance of transient coronal holes and the detection of the CME in coronal images is consistent with them being different manifestations of the same phenomena, but a precise estimate of the CME start time is difficult, since the events studied here were relatively far from the solar limb. They have large projection effects and the CMEs appear faint in Mk4 polarized images of the low corona, which are crucial to determine the initial acceleration of the CME. We tried to account for projection effects since they are important in determining the correct trajectories. This implies making assumptions on the direction in which the CME propagates. For events near disk center, even with Mk4 observations, it is hard to determine the CME acceleration, and an underestimate of the initial acceleration will result in a later start for the CME. Within these observational limits, the CME seems to precede the formation of the transient coronal holes by several minutes and, in one case, by almost an hour. The relationship with the filament eruption is more complex. The filament eruption can precede or follow the CME and transient coronal holes, and we found two cases where no filament eruption could be established with confidence.

We have searched for a possible signature of transient coronal holes in the Hα images, but we have found no evidence of them. The Hα line intensity is largely controlled by photospheric and chromospheric radiation, but coronal contribution to this line is weak. This can explain why transient coronal holes (or coronal holes in general) are not visible at this wavelength.

The high cadence of the MLSO He I 1083 nm observation allowed us to follow the formations of the transient coronal holes accurately. We were able to determine when the holes begin to form and reach their maximum contrast level. The formation time typically varies from 20 minutes to about an hour, as illustrated by the light curves in § 4. We could also detect other transient phenomena, such as the passage of waves, rapid flaring, as well as changes in filaments and active regions at significant distances from the CME source. An interesting finding is the existence in three events of a relatively large region, away from the main two-ribbon flare and partially overlapping the region where the transient coronal holes form, which brightens in Hα and darkens in He I 1083 nm. There is not a clear velocity signal associated with these phenomena, so they appear to be short-lived flares preceding the formation of the coronal holes. Some of these transient events last only a few minutes and are not always noticeable in EIT because of its cadence. We searched the *TRACE* database, to see if the short-lived flaring was detected by the *TRACE* instrument. Unfortunately, for the events in Table 1 covered by the *TRACE* observations, the *TRACE* field of view was centered on the site of the main flare and did not include the secondary flaring or the regions of the transient coronal holes.

For the cases studied here, the intensity contrast of transient coronal holes in the Fe XII 19.5 nm and He I 1083 nm line is similar to that found in longer lived coronal holes. Typical values for the photospheric magnetic flux within the regions where the transient coronal holes forms are 7–12 Mx cm^{-2}, i.e., of the same order of the magnetic flux found within other coronal holes, that usually ranges between 5 and 15 Mx cm^{-2} (Harvey & Recely, 2002; G. de Toma et al. 2005, in preparation). Preliminary analysis of seven other cases, not included in this study, suggests that these are common values for transient coronal holes. However, it is possible that compact, transient coronal holes that form within an active region plage have stronger magnetic flux than the ones reported here. We found one case, on 1999 July 23, when a transient coronal hole partly

TABLE 1

SUMMARY OF ACTIVITY AT TIMES OF TRANSIENT CORONAL HOLES

Date	Transient Coronal Holes	Near/Within AR	Hα Filament Eruption (based on velocity data)	Two-Ribbon Flare (start/peak)	Secondary Flaring	Activation of Other ARs	Coronal Wave	CME Velocity
1999 Jul 23	Start at 2008 UT	AR 8636 (beta-gamma)	1658–2146 UT, 1840–1858 UT[a]	1833/2006 UT	No	No	No	Moderate
2000 Jan 28.....	Start at 2014 UT	AR 8841 (beta)	Possible filament eruption	1942/2009 UT	Yes	No	Probable	Fast
2000 Jan 31.....	Start at 1949 UT	AR 8851 (beta)	No clear filament eruption[b]	In progress[b]	No	No	No	Moderate
2000 Nov 25.....	Start at 1827 UT	AR 9236 (beta-gamma)	1715–1755 UT, 1838–2019 UT	1837/1844 UT[c]	Yes	No	Yes	Fast
2001 Jan 20.....	Start at 1847 UT	AR 9313 (beta)	1756–2015 UT	1837/1853 UT	Yes	Yes	Yes	Fast
2002 Dec 19.....	Start at 2149 UT	AR 10229 (beta-gamma)	2015–2100 UT	1834/2149 UT	Yes	Yes	Yes	Fast

NOTES.—The table gives the start time of the transient coronal holes and their association with other manifestations of the CME for the six events studied. The start time of transient coronal holes is based on when they first became visible in either Fe XII 19.5 nm or He I 1083 nm. The time of the filament eruption is based on MLSO He I velocity data, while the start and peak times of the flare are based on MLSO Hα data. Secondary flaring refers to any flaring associated with the eruption, outside of the active region and not part of the main two-ribbon flare. We define activation of nearby active regions as a sudden change in the active region contrast as observed in He I 1083 nm and Hα data that appears to be connected with the eruption. Coronal waves are identified in EIT data, and CMEs are divided into fast and moderate depending on whether their final velocity, corrected for projection effects, is above 1000 km s^{-1} or between 500 and 1000 km s^{-1}.

[a] Multiple filament eruptions. Velocity peaks at 1840–1858 UT.

[b] The event had already started at the beginning of the MLSO observing day.

[c] The flare peak is based on *GOES* X-ray data. MLSO Hα data were not available during flare peak.

overlapped the plage area. For this case the average photospheric magnetic flux within the transient coronal hole region was about 36 Mx cm^{-2}.

All the events discussed here occurred during the maximum phase of solar cycle 23, and they differ in some characteristics from earlier cases of EUV dimmings detected with EIT during the years 1997–1998 (Zarro et al. 1999; Thompson et al. 1998, 2000). Some of the early dimmings formed close to the flare site and had a more symmetric, two-lobed shape. On the contrary, the cases discussed here often have an irregular, nonsymmetric shape and cover a large area that can extend to significant distance from the flaring active region. For example, in the 2002 December 19 event, there are three elongated transient coronal holes that form south of the active region, over an area of about 20° in latitude and 25° in longitude; while in the 2000 November 25 event, a preexisting coronal hole next to the flaring active region, but not directly adjacent to it, significantly increases in size. The symmetry and size of transient coronal holes likely depends upon the distribution and intensity of the magnetic field within and around the source region of the CME. In all the cases reported here, the active regions where the CME originates are far from being simple dipoles and the global topology of the solar magnetic field is more complex then during the years 1997–1998. This complexity is likely to affect how the CME evolves, and, consequently, the appearance of the transient coronal holes. As originally suggested by Thompson et al. (2000), we expect more symmetric, two-lobed transient coronal holes to occur in simple, bipolar active regions during the rising phase of the cycle, but that they will be less common at solar maximum.

Our study covered six cases of transient coronal holes during the period 1999–2002 that were associated with CMEs originating in active regions. A larger statistical study, which covers different phases of the solar cycle and includes transient coronal holes associated with polar crown and other filament eruptions away from active regions, is necessary to better understand the relationship among transient coronal holes, the CME itself and the other surface manifestations of the CME. We have shown that MLSO observations in the He I 1083 nm line are useful to study short-lived phenomena, such as transient coronal holes, rapid flaring and waves occurring at the CME onset. Full-disk, high-cadence observations in the EUV, such as the ones from SDO, will provide even more information on the early phase of CMEs.

We acknowledge our dearest friend and colleague Karen Harvey, who died in 2002. She was a pioneer in the use of He I 1083 nm observations to study CME signatures on the solar disk and coronal holes. She warmly encouraged us to start this study. The Mauna Loa Solar Observatory (MLSO) is operated by the High Altitude Observatory (HAO) in Boulder, Colorado. HAO is part of the National Center for Atmospheric Research operated by the University Corporation for Atmospheric Research under sponsorship of the National Science Foundation This research has been supported by NASA grant W-19950.

REFERENCES

Andretta, V., & Jones, H. P. 1997, ApJ, 489, 375
Avrett, E. H., Fontenla, J. M., & Loeser, R. 1994, in IAU Symp. 154, Infrared Solar Physics, ed. D. M. Rabin, J. T. Jefferies, & C. Lindsey (Dordrecht: Kluwer), 35
Brueckner, G. E., et al. 1995, Sol. Phys., 162, 357
Delaboudinière, J. P., et al. 1995, Sol. Phys., 162, 291
Delannée, C., Delaboudinière, J. P., & Lamy, P. 2000, A&A, 355, 725
Dere, K. P., et al. 1997, Sol. Phys., 175, 601
———. 2000, Sol. Phys., 195, 13
Elmore, D., et al. 1998, Appl. Opt., 37, 4270
Fontenla, J. M., Avrett, E. H., & Loeser, R. 1993, ApJ, 406, 319
Gibson, S. E., & Low, B. C. 2000, J. Geophys. Res., 105, 18187
Gilbert, H. R., & Holzer, T. E. 2004, ApJ, 610, 572
Gilbert, H. R., Holzer, T. E., Thompson, B. J., & Burkepile, J. T. 2004, ApJ, 607, 540
Giovanelli, R. G., Hall, D. N., & Harvey, J. W. 1972, Sol. Phys., 22, 53
Gopalswamy, N., & Hanaoka, Y. 1998, ApJ, 498, L179
Gopalswamy, N., & Thompson, B. J. 2000, J. Atmos. Sol.-Terr. Phys., 62, 1457
Handy, B. N., et al. 1999, Sol. Phys., 187, 229
Hansen, R. T., Garcia, C. J., Hansen, S. F., & Yasukawa, E. 1974, PASP, 86, 500
Harra, L. K., & Sterling, A. C. 2001, ApJ, 561, L215
Harrison, R. A., Bryans, P., Simnett, G. M., & Lyons, M. 2003, A&A, 400, 1071
Harrison, R. A., & Lyons, M. 2000, A&A, 358, 1097
Harvey, J. W., & Livingston, W. C. 1994, in IAU Symp. 154, Infrared Solar Physics, ed. D. M. Rabin, J. T. Jefferies, & C. Lindsey (Dordrecht: Kluwer), 59
Harvey, J. W., & Sheeley, N. R. 1979, Space Sci. Rev., 23, 139
Harvey, K. L., McAllister, A., Hudson, H. S., Alexander, D., Lemen, J. R., & Jones, H. P. 1996, in ASP Conf. Ser. 95, Solar Drivers of Interplanetary and Terrestrial Disturbances, ed. K. S. Balasubramanian, S. L. Keil, & R. N. Smartt (Dordrecht: Kluwer), 100
Harvey, K. L., & Recely, F. 1984, Sol. Phys., 91, 127
———. 2002, Sol. Phys., 211, 31
Howard, T. A., & Harrison, R. A. 2004, Sol. Phys., 219, 315
Hudson, H. S., Acton, L. W., & Freeland, S. L. 1996, ApJ, 470, 629
Hudson, H. S., & Cliver, E. W. 2001, J. Geophys. Res., 106, 25199
Hudson, H. S., Lemen, J. R., St. Cyr, O. C., Sterling, A. C., & Webb, D. F. 1998, Geophys. Res. Lett., 25, 2481
Hudson, H. S., & Webb, D. F. 1997, in Coronal Mass Ejections, ed. N. Crooker, J. Joselyn, & J. Feyman (Geophysic. Monogr. 99; Washington, DC: AGU), 27
Hundhausen, A. J. 1997, in Cosmic Winds and Heliosphere, ed. J. R. Jopikii, C.P. Sonett, M. S. Giampapa (Tucson: Univ. Arizona), 259
———. 1999, in The Many Faces of the Sun, ed. K. T. Strong, et al. (New York: Springer), 143
Jones, H. P. 1994, in IAU Symp. 154, Infrared Solar Physics, ed. D. M. Rabin, J. T. Jefferies, & C. Lindsey (Dordrecht: Kluwer), 498
Kahler, S. W., & Hudson, H. S. 2001, J. Geophys. Res., 106, 29239
MacQueen, R. M., Blankner, J. G., Elmore, D. F., Lecinski, A. R., & White, O. R. 1998, Sol. Phys., 182, 97
Mandrini, C. H., Pohjolainen, S., Dasso, S., Green, L. M., Démoulin, P., van Driel–Gesztelyi, L., Copperwheat, C., & Foley, C. 2005, A&A, in press
Manoharan, P. K., van Driel–Gesztelyi, L., Pick, M., & Démoulin, P. 1996, ApJ, 468, L73
McCabe, M. K., & Mickey, D. L. 1981, Sol. Phys., 73, 59
Moses, J., et al. 1997, Sol. Phys., 175, 571
Neupert, W. M., Thompson, B. J., Gurman, J. B., & Plunkett, S. P. 2001, J. Geophys. Res., 106, 25215
Penn, M. J., & Jones, H. P. 1996, Sol. Phys., 168, 19
Penn, M. J., & Kuhn, J. R. 1995, ApJ, 441, L51
Plunkett, S. P., Thompson, B. J., St. Cyr, O. C., & Howard, R. A. 2001, J. Atmos. Sol.-Terr. Phys., 63, 389
Rust, D. M. 1983, Space Sci. Rev., 34, 21
Rust, D. M., & Hildner, E. 1976, Sol. Phys., 48, 381
Schmidt, W., Knölker, M., & Westendrop Plaza, C. 1994, A&A, 287, 229
Sterling, A. C., & Hudson, H. S. 1997, ApJ, 491, L55
Sterling, A. C., Hudson, H. S., Thompson, B. J., & Zarro, D. M. 2000, ApJ, 532, 628
Thompson, B. J., Cliver, E. W., Nitta, N., Delannée, C., & Delaboudinière, J. P. 2000, Geophys. Res. Lett., 27, 1431
Thompson, B. J., Plunkett, S. P., Gurman, J. B., Newmark, J. S., St. Cyr, O. C., & Michels, D .J. 1998, Geophys. Res. Lett., 25, 2465
Vršnak, B., Warmuth, A., Brajša, R., & Hanslmeier, A. 2002, A&A, 394, 299
Watanabe, T., Kojima, M., Kozuka, Y., Tsuneta, S., Lemen, J. R., Hudson, H., Joselyn, J. A., & Klimchuk, J. A. 1994, in X-Ray Solar Physics from Yohkoh, ed. Y. Uchida et al. (Tokyo: Universal Academy Press), 207
Webb, D. F. 2000, J. Atmos. Sol.-Terr. Phys., 62, 1415
Webb, D. F., McIntosh, P. S., Nolte, J. T., & Solodyna, C. V. 1978, Sol. Phys., 58, 389
White, O. R. 1964, ApJ, 139, 1340
White, O. R., & Wilson, P. R. 1966, ApJ, 146, 250
Zarro, D. M., Sterling, A. C., Thompson, B. J., Hudson, H. S., & Nitta, N. 1999, ApJ, 520, L139
Zirin, H. 1975, ApJ, 199, L63
———. 1988, Astrophysics of the Sun (Cambridge: Cambridge Univ. Press)